CATRINA (2024), 31 (1):25-39

Insights into Using a Schiff Base as a Corrosion Inhibitor for Carbon Steel in HCl Medium: Experimental and Theoretical Approaches

Amal R. El Tohamy[1*], M. M. Kamel[1*], A. Aboelmagd[1], S. M. Rashwan[1], A. S. Fouda[2], M. K. Awad [3], F. M. Atlam[3]

[1]Department of Chemistry, Faculty of Science, Suez Canal University, Ismailia, 41522, Egypt
[2]Department of Chemistry, Faculty of Science, Mansoura University, Mansoura, 35516, Egypt
[3]Department of Chemistry, Faculty of Science, Tanta University, Tanta, 31527, Egypt

Received October 5, 2023, accepted January 18, 2024

ABSTRACT

In an aqueous environment, the corrosion of metals or alloys is often inhibited by the application of organic inhibitors. On carbon steel (CS), N, N′-bis (salicylidene) butylene-1,4-diamine (SB) was investigated for its anticorrosive properties. With the use of potentiodynamic polarization (PDP), electrochemical impedance spectroscopy (EIS), and weight loss (WL) measurements, corrosion behavior in the temperature range of 298-333 K, both with and without the SB inhibitor, was predicted. A maximal inhibitory effectiveness of 84.0% was observed in half molar HCl at 298 K, and it rises as SB (50-300 ppm) concentration increases. The variation in kinetic and thermodynamic properties of SB on CS indicates mixed adsorption (physisorption and chemisorption). The polarization curves indicate its mixed kind of inhibition activity followed by the Langmuir adsorption isotherm. The experimental results are supported by density functional theory (DFT) and Monte Carlo (MC) simulations, indicating the potential corrosion inhibition behavior of SB on CS in acidic environments. SEM and EDX analyses revealed the development and adsorption of a continuous layer at CS in the presence of the SB chemical. The quantum characteristics of SB supported its efficacy as an inhibitor.

Keywords: Corrosion inhibition; Carbon steel; HCl; Schiff base; Quantum chemical calculation.

INTRODUCTION

Corrosion is the spontaneous degradation of metallic materials in an aggressive environment. Corrosion continues to be a major global scientific issue with terrible effects for the metallurgical, chemical, food manufacturing, oil industries, and possibly human life (Kumar *et al*., 2022; Verma *et al.*, 2017). Metal components are cleaned using pickling processes, which remove contaminants including oil, stains, oxide layers, and corrosion products from the material's surface. Acids such as HCl, H_2SO_4, H_3PO_4, HF, and organic acids like acetic acid, citric acid, and oxalic acid can be used individually or in mixtures for this method. Without inhibitor usage, the corrosive effect of acid on parts will lead to a remarkable amount of metal loss during the pickling process (Nabatipour *et al.*, 2020; Tang, 2019). Organic inhibitors are the most effective compounds because they have one or more polar groups (O, N, P, and S atoms and π-electrons). They are successful in preventing corrosion by adsorbing on the surface of the metal and creating a barrier film (Al-Baghdadi *et al*., 2021; Bahaa El-Dien *et al.*, 2019). A class of organic compounds known as Schiff's bases is synthesized by the condensation of aliphatic or aromatic amines with aldehydes. Recently, they have been found to be excellent corrosion protectors for CS in several environments, especially sulphuric and hydrochloric acids (Abdallah *et al.*, 2019; Alwan, 2018; Chen *et al.*, 2021; Hashemi *et al.*, 2021; Jamil *et al.*, 2018; Wang, 2021; Zhang *et al.*, 2019). A few scientists attributed the inhibition efficacy to the existence of vacant π* orbitals in Schiff base molecules. Since these orbitals allow the backward supply of electrons from metal d-orbitals, the inhibitor-metal bond is stabilized. Schiff bases and their metal complexes have important uses in medicine as antibacterial, antioxidant, and anti-inflammatory agents, as well as in industry as corrosion inhibitors (Liang *et al* (2019). Hegazy *et al* (2021) investigated the azomethine compound (6E, 7E)-N1, N 6-bis (1-methylpyrrolidin-2-ylidene) hexane-1, 6-diamine as an anti-corrosion agent for CS in 0.5 M H_2SO_4 solution. They claimed that by raising the concentration of the synthetic inhibitor the inhibition effectiveness improved. 2-(2-oxoindolin-3-ylidene) (OHB), an Isatin Schiff base, was synthesized and described by Al-Amiery *et al*., (2022). They evaluated that the OHB suppressed the corrosion of mild steel specimens in 1 M HCl. The experimental findings demonstrated that OHB has good corrosion inhibition with a maximum corrosion inhibition efficiency of 96.7% at a concentration of 0.5 mM and 303 K. Natash Mary *et al*., (2022) evaluated the ability of 2 Schiff bases derived from triazole, 4-[(furan-2-ylmethy-lidene)-amino]-5-methyl-4H-1,2,4-triazole-3-thiol and 4-[(chlorobenzylidene)amino] -5-methyl-4H-1,2,4-tria-zole-3-thiol, to suppress the dissolution of steel by a 2:1 mixture of HCl and H_2SO_4. The inhibition efficacy of both derivatives increased with increasing temperature and derivative concentration. Al-Najjar and Al-Baitai (2022) synthesized and tested a new imidazole derivative known as (N, N'E, N'E)-N, N'-(thiophene-2,5diylbis (methanylylidene) bis (1H-

* *Corresponding author e-mail: amal_refaat@science.suez.edu.eg*

benzo[d]imidazol-2-amine) as corrosion inhibitors in a 0.1 M HCl solution. According to their findings, the mitigation efficacy rose when the inhibitor concentration was increased but decreased as the temperature was raised. The highest inhibition efficacy was found to be 96% at 0.5 mM of the prepared inhibitor. N'-[4-(dimethylamino) benzy-lidene]-4-hydroxybenzohyd-razide, a Schiff base, was studied by Kumari and Lavanya (2021) to find out how it affected the inhibition of corrosion of mild steel in HCl solution. Kinetic and thermodynamic parameters confirmed the ability of the synthesized inhibitor to protect the mild steel. The experimental results indicated that the examined chemical seemed to have a powerful anti-corrosion capability. Zhuang *et al*. (2021) examined imidazoline Gemini surfactants as corrosion inhibitors for carbon steel X70 in NaCl solution. It was observed that the higher concentration of the Gemini imidazoline surfactant, the better the inhibition effect, which reached 75.45% at a concentration of 500 mg L^{-1}. The corrosion inhibition activity of three Schiff bases, benzylidene-pyridine-2-yl-amine (BPA), (4-methylbenzylidene)-pyridine-2-ylamine (4CH3-BPA), and (4-chloro-benzylidene)-pyridine-2-yl-amine (4ClBPA), was investigated by Kaur *et al.* (2021). The order of corrosion inhibition activity for these Schiff bases was found to be in the following order: 4Cl-BPA > 4CH3-BPA > BPA. Both chloride and methyl substituents on the benzene ring contribute to an increase in electron density, thereby enhancing the interaction between the Schiff base and the metal surface.

The corrosion-inhibition properties of several Schiff bases based on ferrocene, such as Ferrocenyl Schiff bases 4,40-(ethane-1,2-diylbis (oxy) bis (4,1-phenylene) bis (methaneylylidene) bis (azaneylylidene) bisferrocene (Fcua), 4,40-(ethane-1,2-diylbis(oxy) bis (2-methoxy-1,4-phenylene) bis (methaneylylidene) bis (azaneylylidene) bisferrocene (Fcub) and 4,40-(ethane-1,2-diylbis(oxy) bis (2-ethoxy-1,4-phenylene) bis (methaneylylidene) bis (azaneylylidene)) bisferrocene (Fcuc), were investigated on an Al alloy in an acidic medium (Nazir *et al* 2020). The assessed inhibition efficiencies were 92, 94 and 96 for Fcua, Fcub and Fcuc, respectively using EIS tests. Schiff bases, namely 3-(4-hydroxybenzylidene) amino)-2-methylquina-zolin-4(3H)-one (BZ3) and 3-(4-(dimethylamino) benzylidene) amino)-2-methylquin-azolin-4(3H)-one (BZ4), were employed as highly efficient inhibitors of mild steel corrosion by corrosive acid (Jamil *et al*., 2018). Inhibition efficiencies of 96 and 92 were achieved with BZ4 and BZ3, respectively. The inhibition performance of 1-hydralazinophth-alazine (HPZ) (1), and synthesized1-(2-[(5-methyl-furan-2-yl) methylene)] hydrazono) phthalazine (MFHPZ) (2), 1-(phthalazin-1(2H)-one) [(pyridin-2-yl) ethyli-dene] hydrazone (ACPHPZ) (3) and (2-acetylthiophene hydrazono) phthalazine (ACTHPZ) (4) has been investigated for mild steel in 1 M HCl (Njong *et al*., 2018). Compound 4 showed a maximum inhibition efficiency of 93% at 5.0×10^{-3} M concentration.

Three new bis-Schiff bases: 1,10 -(2,20 -dibromo-[1,10 -biphenyl]-4,40-diyl) bis (N-phenylmethanimine) (BNSB01), 1,10-(2,20-dibromo-[1,10 biphenyl]-4,40-diyl) bis (N-(4-bromophenyl) methan-imine) (BNSB02) and 4,40 -(2,20-dibromo-[1,10 -biphenyl]-4,40-diyl) bis(methanylylidene)bis(azanylyli-dene)) diphenol (BNSB03) were synthesized by Arshad *et al*., (2020). They used them as corrosion inhibitors for mild steel specimens in 0.5 M HCl solution. The findings showed that BNSB02 had the highest inhibition efficiency (90.3%), followed by BNSB03 (87.9%), and BNSB01 (85.6%).

The objective of this study is to synthesize and characterize N,N'-bis(salicylidene)-butylene-1,4-diamine Schiff base (SB) and evaluate its performance as a corrosion inhibitor for carbon steel (CS) in a 0.5 M HCl solution. The corrosion assessment is conducted through WL (weight loss), EIS (electrochemical impedance spectroscopy), and PDP (potentiodynamic polarization) methods. SEM (scanning electron microscopy) and EDX (energy-dispersive X-ray spectroscopy) techniques were employed to examine the morphology and composition of the CS surface. Moreover, thermodynamic and activation parameters were calculated to provide further insights. Additionally, MC (Monte Carlo) simulation and DFT (density functional theory) were utilized to elucidate the interaction between SB molecules and the CS surface.

MATERIALS AND METHODS

Experimental methods

Materials and solutions

Carbon steel of the following weight percentages was utilized in all experiments: C 0.201, Mn 0.602, P 0.041, Si 0.0031, and Fe, the rest. The materials used are salicylaldehyde, 1, 4 di-amino butane, hydrochloric acid (AR acid 36%), ethanol; all purchased from Loba Chemie company and were used without further purification. Pt and Ag/AgCl were employed as counter and reference electrodes, respectively.

Synthesis of N, N′-bis(salicylidene)butylene-1,4-diamine (SB)

The inhibitor SB was synthesized as per the general procedure by refluxing salicylaldehyde (4.2 mL, 4 mmol) with 1, 4 - diamino butane (2 mL, 2 mmol) in ethanol for 4 hours and characterized using the ^{1}HNMR spectroscopic method. The structure of the synthesized compound (SB) is shown below:

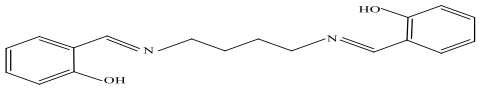

N, N′-bis(salicylidene)butylene-1,4-diamine (SB)
Mol. Formula: $C_{18}H_{24}O_2N_2$, Mol. Wt.: 384.56.

WL method

The WL experiments were conducted by immersing the test specimens in a test solution (50 ml, 0.5 M HCl) with varying concentrations (50 to 300 ppm) of the prepared compound for 3 hours at temperatures ranging from 298 to 333 K. The surface area of the CS that was

exposed to the acidic solution was 9 cm^2 (3×3 cm). The polished coupons were weighed prior to immersion in the acid solution. After exposure, the samples were treated with a pickling solution of HCl (1:1) containing $SnCl_2$ and $SbCl_3$ to remove corrosion products (Hegazy *et al*., 2012). Subsequently, they were rinsed with a 5% $NaHCO_3$ solution to neutralize the acidity before final weighing.

Electrochemical techniques

Electrochemical measurements were conducted with an OrigaLys Potentiostat-OGS 100 and a typical electrolytic cell equipped with three-electrodes. The working electrode (WE) was a CS rod, the counter electrode was Pt gauze, and the reference electrode was Ag/AgCl. Prior to the experiments, WE were given 30 minutes to achieve steady-state potential (OCP). The working electrode's surface, which is 1cm^2, was washed with acetone and double-distilled water prior to being abraded with several grades of abrasive materials. The WE potential was automatically changed from -200 to -650 mV vs. Ag/AgCl at scan rate 0.2 mVs^{-1} to conduct the PDP measurements. The Stern-Geary method was employed to compute the current of corrosion for each dose of the SB compound and the blank solution. The experiments were done three times to guarantee accuracy, and all measureements were accomplished at a temperature of 25°C. Employing AC pulses at OCP with amplitude of 10 mV peak to peak, EIS data was determined within the frequency domain of 100 kHz to 50 mHz. EIS graphics are supplied in both Bode and Nyquist forms. A personal computer was utilized to collect the data. Origin 2021 and Microsoft Office 2016 were employed to display, graph, and fit data.

Surface examination

To study the morphology of the CS surface, coupons were submerged in half molar HCl for 72 hours, devoid of and with the Schiff base compound at an optimal concentration of 300 ppm. After that, the coupons were rinsed with distilled water, dried, and mounted onto a spectrometer without any more care. SEM images were established using a BED-C 10 kV, Jeol, equipped with an EDX device for the purpose of examining the surface morphology and structure of the adsorbed film.

Quantum chemistry calculations

Simulations involving quantum chemistry are carried out to explain the mechanism of adsorption and relate the quantum chemical properties with the reported inhibitory efficacy of the examined corrosion inhibitor. The DFT/6-31+G (d) and Monte Carlo (MC) simulations were employed to establish the quantum chemical variables.

RESULTS

Confirmation of the synthetic SB's structure

The ^{1}HNMR spectroscopy

The ^{1}HNMR spectrum of the prepared compound displayed the following signals: a multiple peak between 1.7-7.8 ppm corresponding to the four protons of the two methylene ($NCH_2CH_2CH_2CH_2N$), whereas the four protons of the other methylene (NCH_2CH_2-CH_2CH_2N) appear as a multiplet peak between 3.6-3.7 ppm. Along with the former signals, the eight aromatic protons appear as multiplet signals between 6.85-7.42 ppm; the two azomethine groups' protons (CH=N) appear as a singlet signal at 8.55 ppm; and the broad peak between 13.1-13.9 ppm is attributed to the two protons of the two phenolic OH groups. The ^{1}HNMR spectrum of Schiff base is illustrated in Fig. (1).

Infrared spectroscopy

The IR spectra show the characteristic peaks of the compound at 1275.19, 1498.06, and 1613.37 cm^{-1}, which correlate to (C-O), (C=C) and (C=N) groups, respectively. As shown in Fig. (2), the OH groups have a broad peak between 3740.31 and 3868.68 cm^{-1}.

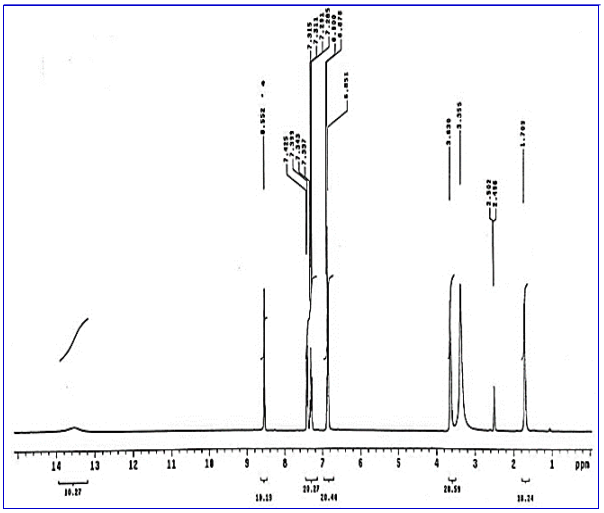

Figure (1): ^{1}H NMR spectrum of N,N′-bis(salicylidene) butylene-1,4-diamine

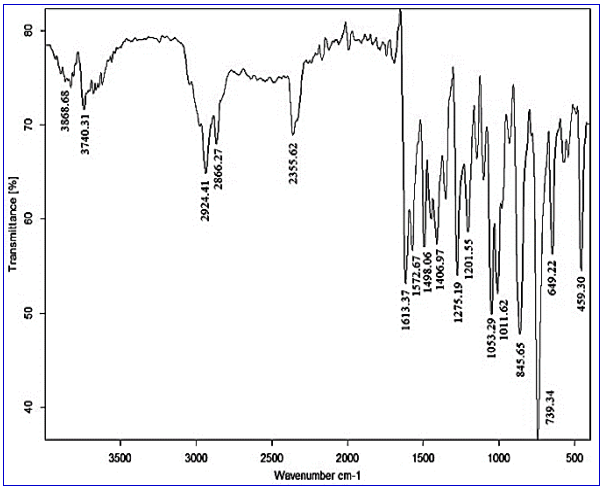

Figure (2): IR spectra of N,N′-bis(salicylidene) butylene-1,4-diamine.

WL measurements

The results of WL measurements are represented in Table (1). The data obtained showed that as the concentration of the SB increases, the corrosion rate (k_{corr}) decreases, and the surface coverage (θ) and inhibition efficiency (% IE) generally increase. The highest concentration of 300 ppm shows a significant decrease

in the corrosion rate (k_{corr}) to 0.28 ± 0.3 (mg cm^{-2} s^{-1}) × 10^{-4}. The surface coverage (θ) increases to 0.84, leading to the highest inhibition efficiency (% IE) of 84.0%. Mean-while, at a concentration of 50 ppm, the measured value of k_{corr} is 0.90 ± 0.2 (mg cm^{-2} s^{-1}) × 10^{-4}, with a corresponding surface coverage (θ) of 0.497 and inhibition efficiency of 49.7%. This suggests that the sub-stance exhibits a concentration-dependent corrosion inhibition effect.

Temperature effect on inhibition efficacy

Data recorded in Table (2) demonstrate a correlation between the concentration of the investigated SB and the corrosion rate at different temperatures. As the concentration of SB increases, the corrosion rate generally decreases. Furthermore, the corrosion rate tends to decrease with increasing temperature for all concentrations. At the lowest concentration of 50 ppm, the corrosion rate of the SB decreases from 0.90 ± 0.2 to 2.64 ± 0.4 (mg cm^{-2} s^{-1}) ×10^{-4} as the temperature increases from 298 to 333 K. Meanwhile, at the highest concentration of 300 ppm the lowest corrosion rates, ranging from 0.28 ± 0.6 to 0.97 ± 0.6 (mg cm^{-2} s^{-1}) ×10^{-4}, across the temperature range, was recorded. The values in the table (3) demonstrate a trend where increasing concentration generally leads to an increase in θ and %IE. As the temperature increases, there is a gradual decrease in θ and %IE for all concentrations.

At the lowest SB concentration, 50 ppm, the values for θ and %IE decrease from 0.497 and 49.7, respectively at 298 K, to 0.478 and 47.8 respectively at 333 K

Table (1): Effect of varying concentrations of the investigated SB on corrosion rate (k_{corr}), surface coverage (θ), and inhibition efficiency (IE) in a 0.5 M HCl solution at 25 °C.

Conc (ppm)	Measured parameters		
	k_{corr} (mg $cm^{-2}s^{-1}$) × 10^{-4}	θ	% IE
Blank	1.80 ± 0.3	-	-
50	0.90 ± 0.2	0.497	49.7
100	0.85 ± 0.1	0.525	52.5
150	0.66 ± 0.1	0.628	62.8
200	0.64 ± 0.2	0.64	64.0
250	0.53 ± 0.2	0.702	70.2
300	0.28 ± 0.3	0.84	84.0

Table (2):Effect of temperature (in Kelvin) and concentration on corrosion rate (k_{corr}) of the investigated SB in a 0.5 M HCl solution.

Conc. (ppm)	k_{corr} (mg cm^{-2} s^{-1}) × 10^{-4}			
	Temperature (in Kelvin†)			
	298	**313**	**323**	**333**
Blank	1.80 ± 0.3	3.00 ± 0.3	3.50 ± 0.5	5.00 ± 0.2
50	0.90 ± 0.2	1.56 ± 0.2	1.81 ± 0.3	2.64 ± 0.4
100	0.85 ± 0.1	1.48 ± 0.4	1.72 ± 0.1	2.53± 0.1
150	0.66 ± 0.5	1.18 ± 0.5	1.38 ± 0.4	2.06 ± 0.3
200	0.64 ± 0.4	1.13 ± 0.4	1.33 ± 0.3	1.98 ± 0.2
250	0.53 ± 0.2	0.94 ± 0.1	1.12 ± 0.1	1.66 ± 0.5
300	0.28 ± 0.6	0.52 ± 0.2	0.63 ± 0.2	0.97 ± 0.6

†Temp in Kelvin= 272.15°C

(Table 3). This trend continues across the concentration range, indicating the influence of both concentration and temperature on the measured values. Therefore, the table provides valuable information on the relationship between concentration, temperature, and the resulting values of θ and %IE.

Activation parameters

The activation parameters for the corrosion of CS in 0.5 M HCl, both without and with different doses of the SB compound, are summarized in Table (4), in which it presents the values of activation energy (E_a^*), enthalpy change (ΔH_a^*), entropy change (ΔS_a^*), and the coefficient of determination (R^2) for different concentrations (ppm). The data indicates that as the concentration increases, there is a slight increase in the activation energy (E_a^*) from 23.32 kJ mol^{-1} for the blank sample to 28.31 kJ mol^{-1} for the 300 ppm concentration. Similarly, the enthalpy change (ΔH_a^*) shows a slight increase from 20.64 kJ mol^{-1} to 25.91 kJ mol^{-1} for the same concentration range. For all the studied concentrations, the entropy change is nearly the same and has negative values. Generally, the coefficient of determination values (R^2) ranging from 0.980 to 0.984 suggest a strong correlation between the variables in the dataset, indicating the reliability of the obtained results.

In summary, the Table provides important insights into the activation parameters for the studied system, highlighting the relationship between concentration and the corresponding activation energy, enthalpy change, and entropy change. Additionally, Fig. (3) illustrates the Arrhenius and transition-state graphs of the SB compound, showcasing the relationship between ln k_{corr} and 1/T, as well as 1n k_{corr}/T and 1/T.

Adsorption study

Analysis of experimental surface coverage data using Langmuir, Freundlich, Flory-Huggins, and Temkin isotherms was conducted to evaluate the adsorption characteristics of the SB inhibitor on the CS surface. The closest match was provided by the Langmuir isotherm model. Langmuir adsorption isotherm, for the SB compound on CS surface (Fig. 4) and data from adsorption of the SB on CS in 0.5 M HCl at varied temperatures are shown in Fig. (4) and Table (5), respectively. The table presents data related to the adsorption study at different temperatures (in Kelvin). The included information, on the slope, intercept, (adsorption constant in mol^{-1}), $-\Delta G^o_{ads}$ (standard free energy of adsorption in kJ mol^{-1}), and the coefficient of determination (R^2), were also discussed. The obtained data shows a trend where the slope, and intercept, values slightly increase; however, K_{ads} values decrease as the temperature change. For example, at 298 K, the slope is 1.05, the intercept is 73.95, and K_{ads} is 1352.26 mol^{-1}. These values gradually increase to 1.10 for the slope, 78.78 for the intercept, and 1269.35 mol^{-1} for K_{ads} at 333 K. Furthermore, the $-\Delta G^o_{ads}$ values decrease as the temperature increases, indicating a decrease in the spontaneity of the adsorption process.

Table (3): Effect of concentration and temperature (in Kelvin) on θ and %IE values of the investigated SB in a 0.5 M HCl solution.

Conc. (PPM)	Temperature (in Kelvin)†							
	298		313		323		333	
	θ	%IE	θ	%IE	θ	%IE	θ	%IE
Blank	-	-	-	-	-	-	-	-
50	0.497	49.7	0.493	49.3	0.488	48.8	0.478	47.8
100	0.525	52.5	0.520	52.0	0.511	51.1	0.501	50.1
150	0.628	62.8	0.616	61.6	0.607	60.7	0.592	59.2
200	0.640	64.0	0.633	63.3	0.622	62.2	0.608	60.8
250	0.702	70.2	0.693	69.3	0.683	68.3	0.671	67.1
300	0.840	84.0	0.830	83.0	0.819	81.9	0.807	80.7

†Temp in Kelvin= 273.15°C

Table (4): Activation parameters and correlation analysis for different concentrations of investigated SB in 0.5 M HCl.

Conc. (ppm)	Activation parameters measured			
	E_a^* (kJ $mol^{-1)}$	ΔH_a^* (kJ $mol^{-1)}$	$-\Delta S_a^*$ (J K^{-1} mol^{-1})	R^2
Blank	23.32	20.64	247.25	0.984
50	24.61	21.97	248.58	0.982
100	24.81	21.98	249.00	0.980
150	25.75	23.11	246.51	0.981
200	25.95	23.35	247.59	0.981
250	26.07	23.45	248.08	0.984
300	28.31	25.91	245.09	0.983

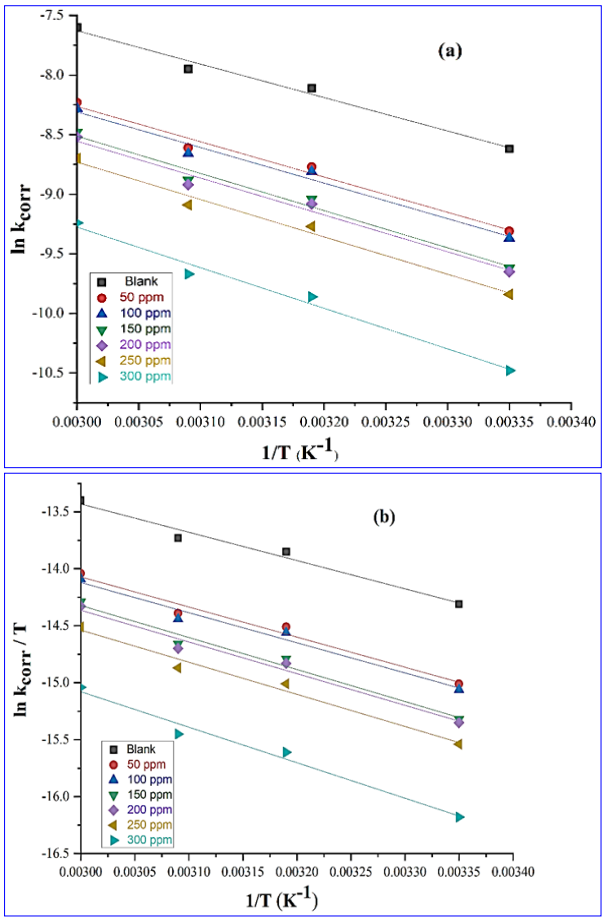

Figure (3): Arrhenius plots (a), and transition-state plots (b) for the corrosion of CS in half molar HCl without and with altered doses of SB.

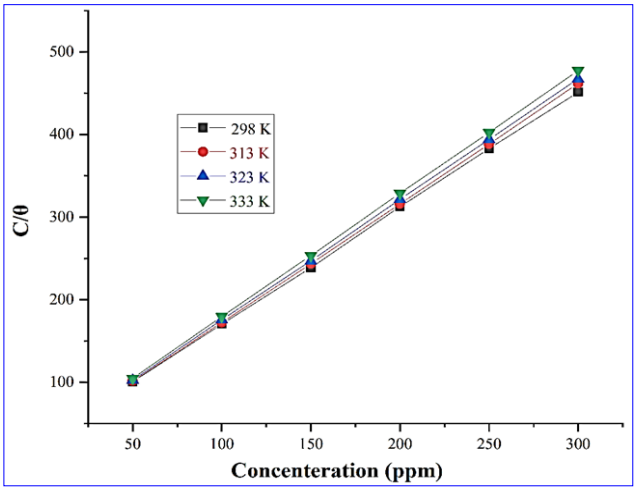

Figure (4): Langmuir adsorption isotherms for CS in half molar HCl without and with SB compound at altered temperatures.

Table (5): K_{ads} and ΔG^o_{ads} of adsorption of the SB on CS in 0.5 M HCl at altered temperatures.

Temp. (K) †	Measured various adsorption parameters				
	Slope	Intercept	K_{ads} (mol^{-1})	$-\Delta G^o_{ads}$ (kJ mol^{-1})	R^2
298	1.05	73.95	1352.26	27.81	0.941
313	1.07	74.76	1337.61	29.18	0.941
323	1.08	76.78	1302.42	30.04	0.939
333	1.10	78.78	1269.35	30.9	0.936

†Temp in Kelvin= 273.15 °C.

The R^2 values in the range of 0.936 to 0.941 demonstrate a strong correlation between the variables in the dataset. Generally, the Table (5) provides important insights into the relationship between temperature and various adsorption parameters such as slope, intercept, K_{ads}, $-\Delta G^{o}_{ads}$, and the coefficient of determination (R^2).

PDP measurements

Effect of the SB compound on the V-I plot of CS in 0.5 M HCl was illustrated in Figure (5). The SB compound retards both the cathodic and anodic reactions. Table (6) presents the values of corrosion current (I_{corr}), corrosion potential (E_{corr}), cathodic Tafel slope (β_c), and anodic Tafel slope (β_a). The data illustrates that the blank sample has a corrosion potential (E_{corr}) of -459.5 mV, while the values decrease with the addition of the SB compound at varying concentrations. The anodic Tafel slope (β_a) also shows a decreasing trend with increasing SB compound concentration, indicating a reduction in the corrosion rate. Conversely, the cathodic Tafel slope ($-\beta_c$) exhibits an increasing trend, suggesting a slower reduction reaction.

The corrosion current (I_{corr}) values decrease as the concentration of the SB compound increases, indicating a decrease in the corrosion rate. This is further supported by the increasing values of inhibition efficiency (%IE) as the SB compound concentration increases. In general, Table (6) provides valuable data on the PDP measurements, demonstrating the effect of the SB compound on various corrosion parameters such as corrosion potential, Tafel slopes, corrosion current and percentage inhibition efficiency.

EIS Measurements

Investigating the corrosion process through electrochemical impedance spectroscopy. The Nyquist and Bode graphs of CS in a blank solution, with and without varying concentrations of SB, presented in Figures (6. and 7), which illustrates the equivalent Randles circuit depicting R_{ct} (charge transfer resistance) and C_{dl} (double-layer capacitance) in parallel, connected to solution resistance (R_s) in series. Table (7) presents data related to the corrosion of CS in 0.5 M HCl at different

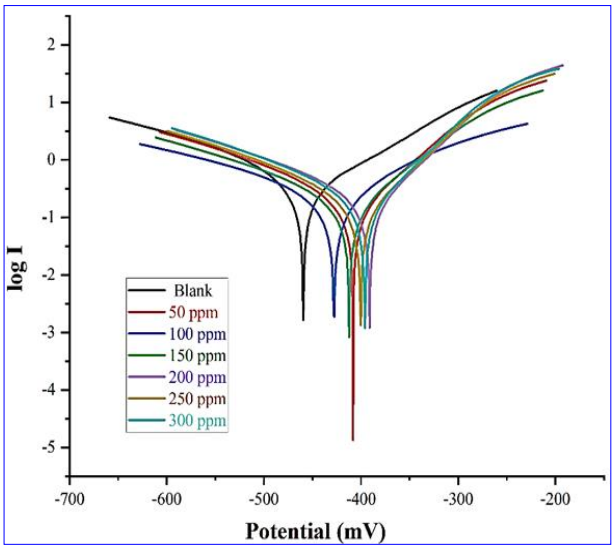

Figure (5): Effect of Different concentrations of SB compound on Tafel plots for CS in 0.5 M HCl at 25 °C: A comparative analysis.

concentrations (ppm) of the SB compound. The table includes information on the charge transfer resistance (R_{ct}) measured in ohms square centimeter, double-layer capacitance (C_{dl}) measured in microfarads, surface coverage (θ), and the percentage inhibition efficiency (%IE).

The data obtained show that the blank sample, without the SB compound, has an R_{ct} value of 43.33 **Ω** cm^2 and a C_{dl} value of 321.4 µF. As the concentration of the SB compound increases, R_{ct} values increase, however, C_{dl} values tend to decrease. This indicates a higher resistance to charge transfer and a decrease in the double-layer capacitance, suggesting an improvement in the corrosion inhibition properties.

Furthermore, the surface coverage (θ) values also increase with increasing SB compound concentration, indicating a higher level of corrosion protection. The percentage inhibition efficiency (% IE) values show a similar trend, with higher values observed at higher SB compound concentrations. In summary, Table (7) provides an important insights into the corrosion behavior of CS in 0.5 M HCl with varying concentrations of the

Table (6): PDP parameters of CS in 0.5 M HCl without and with altered doses of SB compound at 25 °C.

Conc. (ppm)	PDP measurements					
	$-E_{corr}$ (mV)	β_a (mV dec^{-1})	$-\beta_c$ (mV dec^{-1})	$I_{corr}\times10^{-3}$ (A cm^{-2})	θ	%IE
Blank	459.5	146.5	222.8	0.7032	-	-
50	408.2	96.6	209.8	0.3456	0.508	50.8
100	427.9	163.3	260.9	0.3241	0.539	53.9
150	412.2	98.8	200.9	0.2551	0.637	63.7
200	391.1	75.2	173.2	0.2523	0.641	64.1
250	400.5	76.0	148.5	0.1923	0.726	72.6
300	396.1	59.0	83.2	0.1042	0.851	85.1

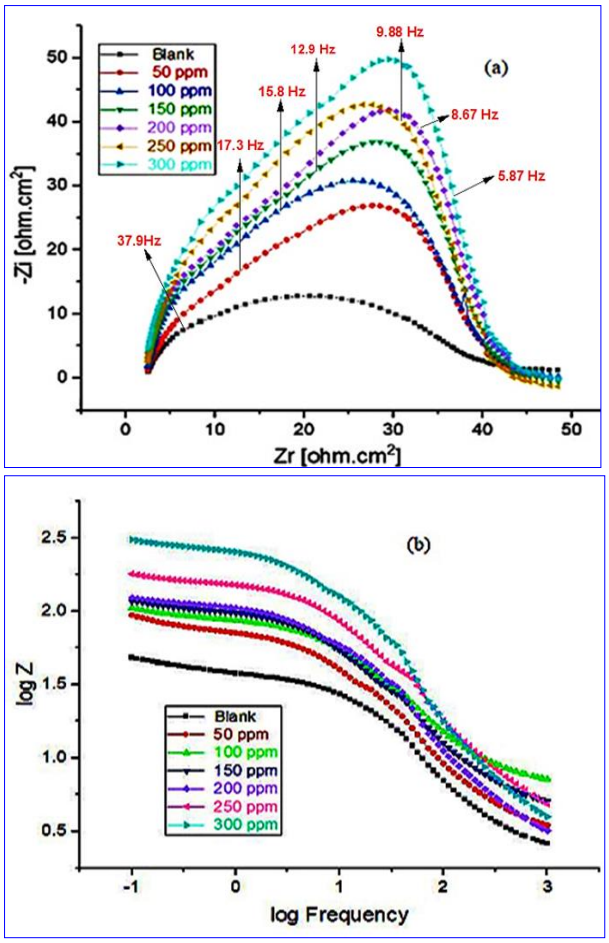

Figure (6): Electrochemical impedance spectroscopy (EIS) analysis of CS corrosion in 0.5 M HCl: Nyquist (a) and Bode (b) plots with varying concentrations of SB at 25 °C.

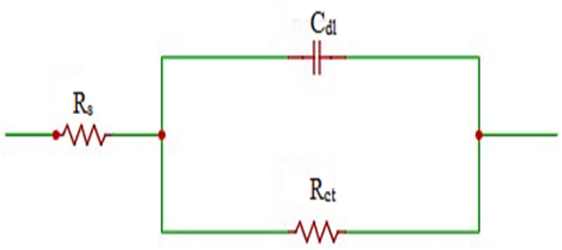

Figure (7): Equivalent circuit model used to fit experimental EIS data.

Table (7): Corrosion inhibition effect of SB compound on CS in half molar HCl: impedance parameters and inhibition efficiency at varying concentrations.

Conc. (ppm)	Measured EIS data			
	R_{ct} (Ω cm^2)	C_{dl} (µF)	θ	%IE
Blank	43.33	321.4	-	-
50	82.75	291.98	0.476	47.6 ± 0.3
100	97.11	242.88	0.553	55.3 ± 0.1
150	108.95	230.8	0.602	60.2 ± 0.4
200	116.63	206.5	0.628	62.8 ± 0.2
250	159.96	153.41	0.729	72.9 ± 0.5
300	280.56	87.46	0.845	84.5 ± 0.1

SB compound. The data highlights the impact of the SB compound on charge transfer resistance, double-layer capacitance, surface coverage of CS, and percentage inhibition efficiency, demonstrating its potential as an effective corrosion inhibitor.

Surface studies

SEM examination

The scanning electron microscopy (SEM) analysis of CS coupons after 72 hrs of exposure in 0.5 M HCl medium at room temperature (25°C) revealed a distinguished difference between samples with and without 300 (ppm) of SB. Severe erosion was observed in the sample without SB, while the presence of SB facilitated the recovery of the steel, as evidenced in Figure (8).

EDX Analysis

To gain deeper insights into the chemical composition, EDX analysis was performed on CS specimens treated in HCl solution both with and without the presence of the SB compound. The resulting EDX spectra of CS specimens in HCl, both without SB and with 300 ppm of the compound, are presented in Figure (9 A and B) respectively.

Exploring the Corrosion Inhibition Mechanism

Quantum chemical calculations play a crucial role in the design and development of corrosion inhibitors. By employing density functional theory (DFT), the distribution of electrons and molecular shape can be accurately determined. In this study, quantum chemical computations were employed to analyze the corrosion characteristics of an inhibitory molecule and its interaction with the metal substrate.

Table (8) presents the quantum chemical parameters of the inhibitor in both protonated and gas forms. Notably, Figure (10) highlights key quantum chemical descriptors such as the energy of the highest occupied molecular orbital (E_{HOMO}) and the energy of the lowest unoccupied molecular orbital (E_{LUMO}). These descryptors provide valuable insights into the reactivity and stability of the inhibitor, shedding light on its potential as an effective corrosion inhibitor.

Molecular electrostatic potentials (MEPs)

Molecular electrostatic potentials (MEPs) are highly valuable for understanding the chemical reactivity. Negative regions in MEPs can be interpreted as nucleophilic centers, while positive regions indicate potential electrophilic sites. Furthermore, the polarization of electron density can be visualized through the electrostatic potential, as illustrated in Figure (11).

These MEPs provide crucial information regarding the distribution of charges and reactivity patterns, aiding in the assessment of the inhibitor's potential interactions and reactivity with the metal substrate.

Monte Carlo Simulation

The advantage of MC simulation is that it runs more quickly than quantum mechanical simulation, reducing money. MC simulations were used to investigate the adsorption behaviour of the CS surface and the type of

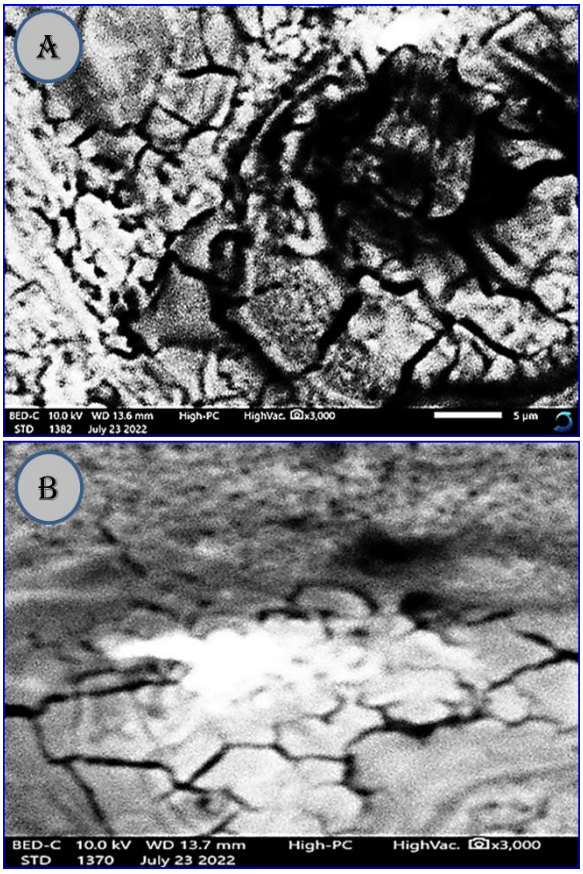

Figure (8): Photomicrograph of CS surface after 72 hrs of immersion in 0.5 M HCl solution. (A), severe corrosion is observed; (B), recovery of the surface is observed after immersion in 300 ppm of the SB compound.

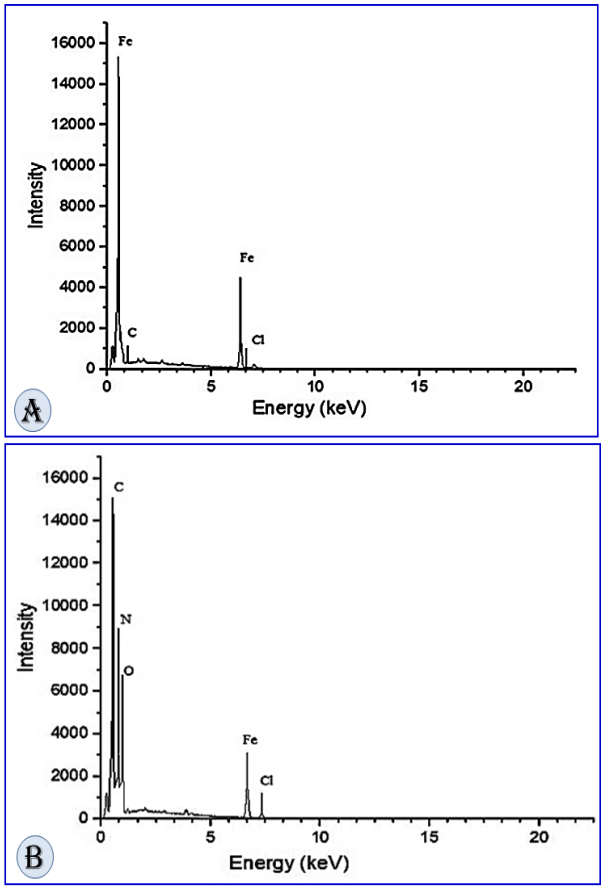

Figure (9): EDX Spectra of CS Specimens. A, immersed in 0.5 M HCl without SB, and B, immersed in 0.5 M HCl with 300 ppm of the SB compound.

Table (8): Quantum chemical parameters of SB in protonated and gas forms.

Compound	Quantum Chemical Parameters	
	Protonated form	Gas form
E_{HOMO}, eV	-4.900	-6.030
E_{LUMO}, eV	-2.521	-3.274
$\Delta E = E_{LUMO} - E_{HOMO}$	2.380	2.760
I	4.900	6.030
A	2.520	3.270
X	3.710	4.650
H	1.190	1.380
Σ	0.840	0.730
Ꞷ	5.790	7.850
DN	1.380	0.850
$\Delta E_{back\text{-}donation}$	-0.300	-0.340
dipole moment *(Debye)*	7.446	8.000

interactions between the SB molecule and the CS surface. Fig. (12) depicts the top and side views of the adsorption modelling of the examined SB chemical on the CS. The outcomes of the MC simulation are shown in Table (9).

DISSCUSION

The weight loss ΔW of the steel sheets is determined from the following equation:

$$\Delta W = W_1 - W_2$$

Where ΔW is the weight loss of the CS coupons, W_1 and W_2 are the coupon weights before and after exposure to the corrosive medium, respectively.

The rate of corrosion, K_{corr}, is estimated based on the preceding equation:

$$K_{corr} = \Delta W / (A \; X \; t)$$

Where ΔW stands for the value of weight loss in *mg*, *A* for the total area per cm^2, and *t* refers to the immersion duration in sec.

As shown in Table (1), the results of CS experiments in 0.5 M HCl acid with and without different quantities of SB inhibitor show that the inhibitor's efficacy at inhibiting growth improves

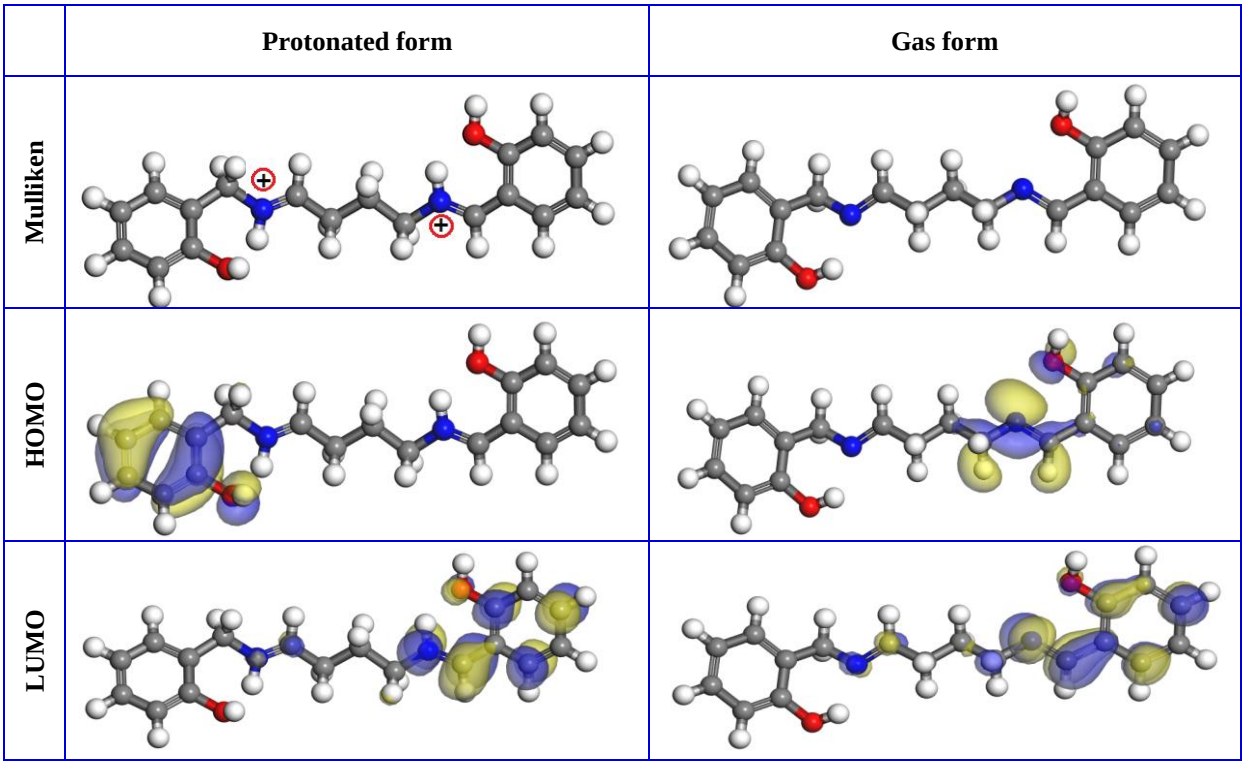

Figure (10): Frontier molecular orbital diagram of the investigated SB and optimized structure

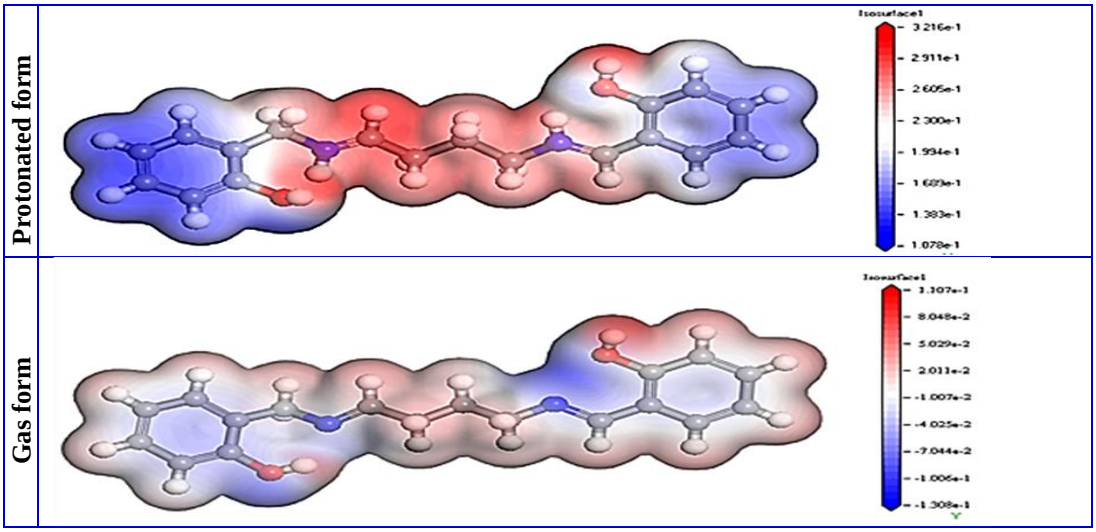

Figure (11): Transparent surface of MEPs of investigated compound in gas and protonated forms.

Table (9): Parameters of molecular dynamic simulation for the studied inhibitor on Fe (1 1 0) surface obtained using the Monte Carlo simulation.

Structure	E_{ads} (kJ mol^{-1})	E_{rigid} (kJ mol^{-1})	E_{def} (kJ mol^{-1})	Compound dE_{ad}/dNi	H_2O dE_{ad}/dNi
Fe (1 1 0) Protonated form	-2133.231	-2054.25	-78.981	-231.31	-11.544
Fe (1 1 0) Gas form	-2058.539	-1989.407	-69.132	-223.64	-9.345

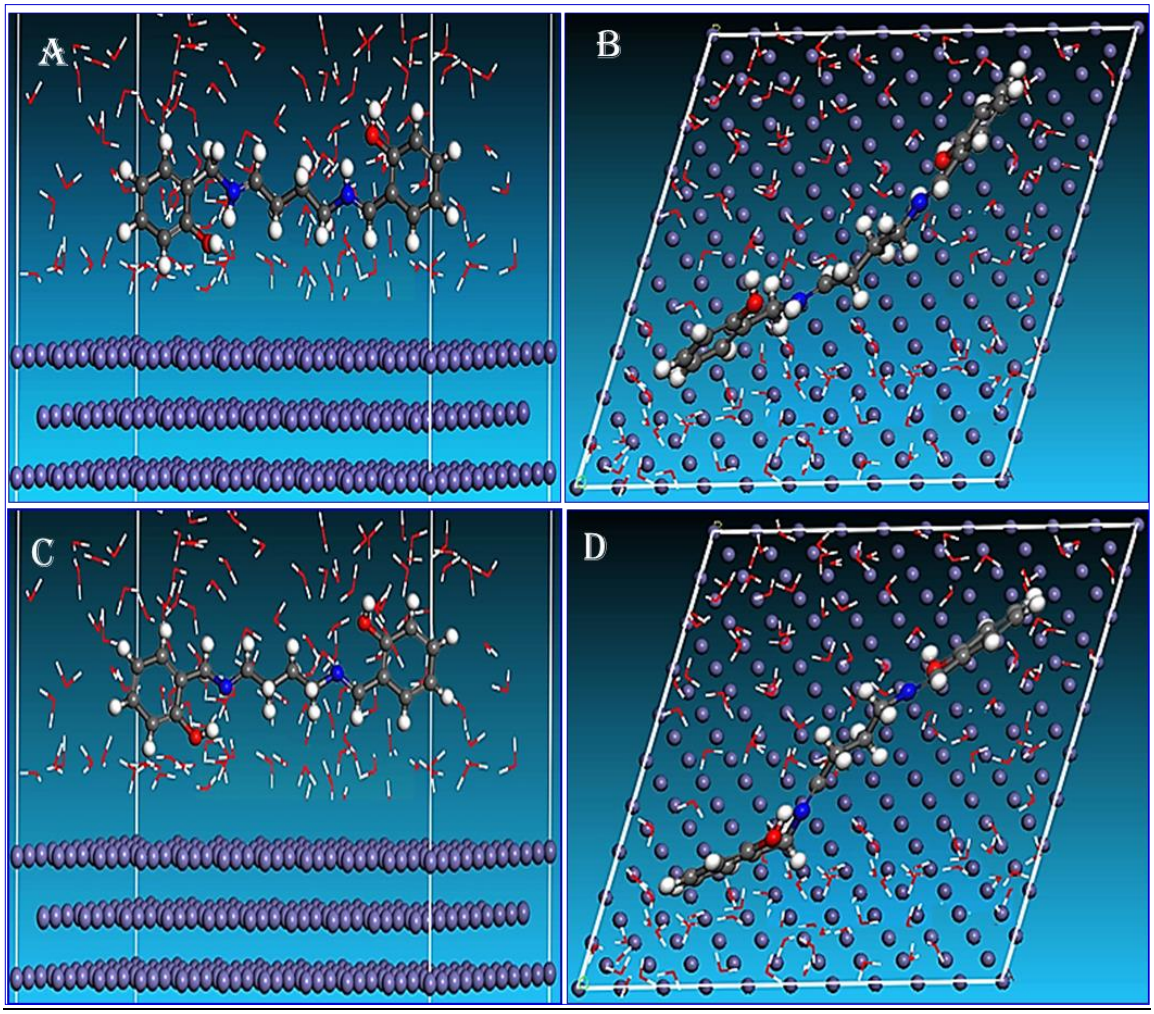

Figure (12): Characterizing the most stable adsorption configuration of the studied inhibitor on Fe (110) surface in the aqueous phase: insights from side view and top view. A and B are side and top view, respectively, of protonated form. C and D are side and top view, respectively, of gas form.

with increasing its concentration in corrosive media. An increase in the SB concentration tends to increase the surface area encased by the adsorbate molecules. These results are parallel to those recorded by Kamel *et al*., (2022a) in which the inhibition efficacy also increases.

Due to numerous changes on the metal surface, it is extremely difficult to predict how temperature will affect the inhibited acid-metal reaction. These modifications could include fast etching, inhibitor desorption, and perhaps inhibitor breakdown or rearrangement. As the temperature rises, without and with distinct doses of the prepared SB, the rate of corrosion of the CS increases quickly as illustrated in Table (2). This may be a result of the accelerated influence of increasing temperature on the rate of electrochemical processes (Kamel *et al*. 2022b; Njong *et al*., 2018). The efficiency of mitigation decreases with increasing temperature. Desorption of the SB molecules from the CS surface is the primary reason for the declining mitigation efficiency values at increasing temperatures.

Thermodynamic parameters are a vital and important approach for understanding inhibitor adsorption behaviour. The activation energy (E_a^*), enthalpy change (ΔH_a^*), and entropy change (ΔS_a^*) of activation for the corrosion of CS in a half molar HCl solution were calculated. To determine the parameters in the non-availability and availability of distinct doses of the SB compound, equations of both Arrhenius and transition-state were applied.

$$k_{corr} = A\ exp\left(\frac{-E_a^*}{RT}\right)$$

$$\ln\left(\frac{k_{corr}}{T}\right) = \left(\ln\left(\frac{k_B}{h}\right) + \left(\frac{\Delta Sa^*}{R}\right)\right) - \frac{\Delta Ha^*}{RT}$$

Where, K_{corr} is corrosion rate, R is gas constant, K_B is Boltzmann's constant, T is the absolute temperature, and h denotes the Planck's constant.

As shown in Fig (3a). The E_a^* value of the CS's corrosion process is determined using the Arrhenius graph, which displays a linear relation with a slope of -E_a^* / R. Table (4) summarizes the findings. For the blank solution, the value E_a^* is 23.32 kJ mol^{-1}. The activation energy rises with increasing SB concentrations because the SB hinders the corrosion process. The SB could precipitate at the CS surface, or a change in the potential difference at the CS-solution interface due to adsorption could be the origin of this variation.

Transition-state graphs show straight lines with slopes of $(-\Delta H_a^*)/(R)$, and intercepts of $(\ln (k_B/h)$ +

(ΔS_a^*/R)), which were used to calculate the values of ΔS_a^* and ΔH_a^* as illustrated in Fig. (3b). The formation of the transition-state requires heat absorption, as evidenced by the positive values of ΔH_a^* (Table 4). The activated complex compound, which is formed in the transition state, appears to be more ordered than the reactants, according to the negativity of ΔS_a^*.

Different adsorption models were studied to evaluate the SB inhibitor's adsorption characteristics on the CS surface. The closest match was provided by the Langmuir isotherm model. The preceding formula (Kaabi *et al*., 2021) is what the Langmuir isotherm is governed by:

$$\frac{C}{\theta} = \frac{1}{K_{ads}} + C$$

Where *C* is the SB concentration, *θ* is the experimental surface coverage, and K_{ads} represents the adsorption process's equilibrium constant.

The Langmuir mode of adsorption is confirmed by the slope values and linear correlation coefficients, R^2, which are both close to one. The intercepts of the straight lines were used to compute the values of K_{ads}. The results show that the value of K_{ads} decreases as temperature rises (Shahabi *et al*., 2019).

The Gibbs free energy for the adsorption process, $\Delta G°_{ads}$, can be computed.

$$\Delta G° = - RT \ln (55.5\ K_{ads})$$

Where *R* is the universal gas constant, *T* is the Kelvin temperature, and 55.5 represent the molar concentration of water (Abdulridha *et al*., 2020). The $\Delta G°_{ads}$ values' negative sign implies that the adsorption of the SB on the CS surface occurs of its own accord.

The literature claims that electrostatic attraction between charged metals and charged molecules can keep $\Delta G°_{ads}$ values at up to 20 kJ mol^{-1} (physisorption). However, values greater than 40 kJ mol^{-1} imply that chemisorption, or transfer of an electron from the inhibitor to the metal surface, may occur (Kaur *et al*., 2021). For the given investigation, the $\Delta G°_{ads}$ varied between -27.81 and -30.90 kJ mol^{-1}. This indicates that the rate of corrosion of CS is drastically reduced by the SB compound through physisorption and chemi-sorption mechanisms (Njong *et al*., 2018).

According to potentiodynamic polarization measure-ments, the corrosion current drops significantly with a rise in SB concentration. The SB inhibits the disintegration of CS in HCl solution. Data in Fig. (5) show the cathodic polarization curves, which exhibit a similar characteristic. This trend indicates that the reaction mechanism of the cathode was unaffected by SB's adsorption at the CS surface. The slopes of the anodic curves, however, vary, indicating that the anodic reaction's mechanism has changed. This suggests that the dissolution process may be strongly hindered by the adsorption of SB at the CS surface. When SB is not present in the corrosive medium, the Cl^- species play a significant role in the corrosion of CS as follow:

$$Fe_{(s)} + Cl^- \rightarrow (FeCl)_{ads} + e$$

$$(FeCl)_{ads} \rightarrow (FeCl)^+ + e$$

$$(FeCl)^+ \rightarrow Fe^{2+} + Cl^-$$

Both H_2 evolution and O_2 reduction are cathodic reactions.

$$4H^+ + O_2 + 4e \rightarrow 2H_2O$$

$$2H^+ + 2e \rightarrow H_2$$

According to the study of Olasunkanmi *et al.* (2016), the effect of the reduction of dissolved O_2 reduction on the CS disintegration mostly occurs at pH > 4. Therefore, in this study, the predominant cathodic reaction is H_2 evolution.

The Nyquist plot's contours haven't changed appreciably, indicating that the reaction mechanism isn't significantly altered by the SB's attachment to the CS's surface, Fig. (6a). For the Bode graph, Fig.(6b), log |Z| and log f have a direct proportional relationship at the medium frequency range. A slope's value gets closer to 1. This demonstrates the capacitive system's suboptimal performance at intermediate frequencies. According to the information provided, the slope must be 1 and the phase angle must be 90 at mediate frequencies to get the ideal capacitive performance. Inhibited solutions have slopes with greater magnitudes than uninhibited ones. This clarifies the examined SB compound's suppressing capabilities in the CS corrosion process.

Charge-transfer resistance (R_{ct}) and double-layer capacitance (C_{dl}) quantities were computed using impedance measurements. Table (7) demonstrates that as SB concentrations increase, the values of the R_{ct} increase as well. Because of this, the SB's presence lowers the rate of corrosion, which raises the effectiveness of inhibition. The %IE was computed using R_{ct} in the equation described below:

$$\%IE = \frac{R_{ct}^o - R_{ct}}{R_{ct}^o} \times 100$$

Where R_{ct} and R^o_{ct} are the charge transfer resistances with and devoid of the SB, respectively. The following relation was used to get the double-layer capacitance magnitude (C_{dl}):

$$C_{dl} = Y_o(\omega_{max})^{n-1}$$

Where $\omega_{max} = 2\pi f_{max}$ and f_{max} is the frequency at which the imaginary impedance attains its highest value.

Increasing the SB concentration causes a decline in C_{dl} values, Table 7. The main cause of this is that SB molecules on the CS surface are slowly exchanging H_2O molecules. The corrosion reaction of CS will be reduced as a result. As the R_{ct} values increase, the rate of CS degradation reduces. The decrease in C_{dl} values is caused by a rise in the electrical double-layer width, and a decrease in the dielectric constant. According to these findings, the SB molecules work by bonding to the metal/solution interface. When adsorbed Cl^- ions interact with SB molecules, adsorption occurs (Hmamou *et al*., 2012).

According to a scanning electron microscopy (SEM)

examination, the CS surface of the specimens that were exposed to the blank solution is highly damaged because of the pitting action of the Cl^- ions, Fig. (8). Meanwhile, the SB compound renders the surface much smoother, and when it adsorbs at the CS surface, it forms a compacted film. These results support the findings of the WL, PDP, and EIS.

EDX analysis of SB on the CS surface indicates that the decrease in the intensity of the Fe peak for the inhibited sample when compared to the blank sample suggests that a protective coating has developed through SB absorption on the CS surface, shielding the CS surface from the corrosive media. The appearance of oxygen, carbon, and nitrogen signals suggests that the SB molecule has been adsorbed at the CS surface, Fig. (9b).

Quantum chemical descriptors, such as energy of the highest occupied molecular orbital (E_{HOMO}) and energy of the lowest unoccupied molecular orbital (E_{LUMO}), are popularly used as shown in Fig. 10. As shown in Table 8, the investigated inhibitor possesses the highest HOMO level energy at -4.90 eV and the lowest LUMO level energy at -2.521 eV in protonated form but in case of gas form has HOMO level energy and LUMO level energy at -6.03 eV and -3.274 eV respectively. This illustrates that the inhibitor in case of protonated form has a higher reactivity than in case of gas form, producing higher inhibitor efficiency. Several studies have reported that lower ΔE values are associated with greater inhibitory efficacy (Negm *et al.*, 2018). Through this result, the investigated protonated compound has a lower energy gap than in gas form which protects the metal from corrosion to a large extent in protonated form (Gao and Liang, 2007; Zhang *et al.*, 2004). An aqueous solution of inhibitor has a dipole moment of 7.44 and 8.0 in protonated and gas form. Strong dipole-dipole interactions with the CS surface are attributed to the inhibitor's high dipole moment.

The quantum parameters connotation with corrosion hindrance were calculated containing ionization potential ($I_p = -E_{HOMO}$), molecular dipole moment (μ), electron affinity ($E_{A=} -E_{LUMO}$), global hardness (η), electronegativity (χ) that are used to compute the electrons transfer from the inhibitor molecule to the metallic atom ΔN, electrophilicity index (ω), softness (σ), and back-donation (ΔE back-donation), was calculated as Koopmans's theorem from (Koopmans, 1934) the next balance:

$$\mu = -\chi = -\frac{I_p + E_A}{2}$$

$$\chi = \frac{I_p + E_A}{2}$$

$$\eta = \frac{I_p - E_A}{2}$$

$$\sigma = \frac{1}{\eta}$$

$$\omega = \frac{\mu^2}{2\eta}$$

$$\omega = \frac{\mu^2}{2\eta}$$

$$\Delta E_{back\ donation} = -\frac{\eta}{4}$$

The calculations of molecular electrostatic potentials revealed that the electrostatic potential of oxygen and nitrogen atoms is negative, indicating that these atoms are the active sites for binding to the metal surface (Fig. 11).

The inhibitor was preferentially adsorbed with most of the heteroatom parallel to Fe, as seen in the top and side views (Fig. 12, top and side panels, respectively). Thus, the surface area of contact between the inhibitor and Fe is increased. Larger molecules have more surface area, which would improve the effectiveness of their inhibition. As seen in Table (9), the inhibitor's negative adsorption energy points to stable/strong adsorption and chemical interaction with Fe (110). As electrons are given to the vacant d-orbitals of iron as well as oxygen and nitrogen atoms, protective coating forms on the metal's surface (Verma *et al*., 2016). Also, we investigated stable adsorption arrangements of the compound under study on Fe in the aqueous phase in gas and protonated forms. As a result, we draw the conclusion that the tested inhibitor would probably create a stable adsorption layer and guard against corrosion on Fe.

As shown in Table (9), in the aqueous phase in gas and protonated forms inhibitor gave high adsorption energy in negative value found during the simulation process. High values of adsorption energy obtained reflect high inhibition efficiency. Fig. (12) shows balance adsorption shapes of the inhibitor's molecules on the Fe surface for protonated and gas forms side view and top view (Khaled et *al.*, 2021).

The inhibition mechanism

The structure, charge distribution within the molecule, and the interaction between the inhibitor and the metal atom are the primary contributors to the corrosion inhibition activity. Schiff bases are present on the surface of the metal in their protonated forms since corrosion essentially only occurs in acidic environments. To begin with, the protonated Schiff bases physically adsorb on the metal surface. The only interactions that take place during the physical adsorption process are electrostatic ones. Following physisorption, chemical adsorption occurs with the metal's unoccupied d-orbital because of the existence of different π-electrons and nonbonding electrons on heteroatoms found on Schiff bases (Jafari *et al.*, 2019).

The metal surface's active sites are covered by the inhibitor after it has been adsorbed there, which slows the rate of corrosion. Figure. (13) provides the proposed process that demonstrates how the Schiff base interacts with the metal surface. The protonated states may contain counterparts with opposing charges that can interact electrostatically. With Cl^- ions, N^+-H can exhibit electrostatic contact or physical adsorption. The phenyl ring's electrons or the unpaired electrons on the nitrogen atoms may interact with unoccupied d-orbitals during the chemical adsorption process.

CONCLUSION

The Schiff base compound SB is synthesized, and its

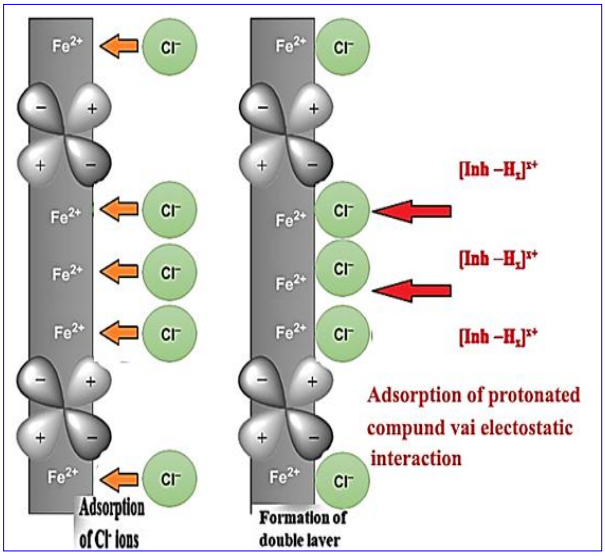

Figure (13): Schematic representation of the physisorption of Schiff bases on CS in half molar HCl solution.

structure is elucidated by (^{1}HNMR) and (FTIR) spectroscopy. The inhibition performance of the synthesized SB towards the corrosion of CS in half molar HCl is investigated. The effectiveness of the inhibition increases as the SB dose increases. The efficiency attains 84% at 300 ppm. The % IE of the synthesized SB slightly declines with rising temperature. The SB acts as a mixed-type inhibitor and follows the Langmuir isotherm model. There is a strong correlation between the data acquired using various approaches (experimental and theoretical), proving its accuracy and reliability. Due to the decreased values of the energy gap for the SB compound, the metal surface is in closer contact with the compound due to electron donation and acceptance. The SB's good inhibitory efficiency was validated by the quantum properties.

ACKNOWLEDGMENT

The authors acknowledge the Chemistry Department at Faculty of Science at Suez Canal University for their cooperation and encouragement during this work.

REFERENCES

ABDALLAH, M., ALFAKEER, M., ALTASS, H.M., ALHARBI, A.M., ALTHAGAFI, I., HASAN, N.F., MABROUK, E.M., 2019. The polarographic and corrosion inhibition performance of some Schiff base compounds derived from 2-amino-3-hydroxypyridine in aqueous media. Egyptian Journal of Petroleum 28, 393-399. https://doi.org/1-0.1016/-j.ejpe.2019.09.002

ABDULRIDHA, A.A., ALBO HAY ALLAH, M.A., MAKKI, S.Q., SERT, Y., SALMAN, H.E., BALAKIT, A.A., 2020. Corrosion inhibition of carbon steel in 1 M H_2SO_4 using new Azo Schiff compound: Electrochemical, gravimetric, adsorption, surface and DFT studies. J Mol Liq 315. https://doi.org/10.1016/j.molliq.2020.113690

AL-AMIERY, A.A., AL-AZZAWI, W.K., ISAHAK, W.N.R.W., 2022. Isatin Schiff base is an effective corrosion inhibitor for mild steel in hydrochloric acid solution: gravimetrical, electrochemical, and computational investigation. Sci Rep 12. https://doi.org/10.1038/s41598-022-22611-4

AL-BAGHDADI, S.B., KADHIM, A., SULAIMAN, G., AL-AMIERY, A.A., ABDUL AMIR, H.K., TAKRIFF, M.S., 2021. Anticorrosion and antibacterial effects of new Schiff base derived from hydrazine, in: Journal of Physics: Conference Series. IOP Publishing Ltd. https://doi.org/10.1088/1742-6596/1795/1/012021

AL-NAJJAR, S.S., AL-BAITAI, A.Y., 2022. Synthesized of Novel Imidazole-derived Schiff Base as a Corrosion Inhibitor of Carbon Steel in Acidic Medium Supported by Electrochemical and DFT Studies. Physical Chemistry Research 10, 179–194. https://doi.org/10.22036/pcr.2021.300569.1955

ALWAN, W.M., 2018. Synthesis, Characterization and the Corrosion Inhibition Study of Two Schiff Base Ligands Derived from Urea and Thiourea and Their Complexes with Cu(II) and Hg(II) Ions, in: Journal of Physics: Conference Series. Institute of Physics Publishing. https://doi.org/10.1088/17426596/10-03/1/012017

ARSHAD, I., SAEED, A., CHANNAR, P.A., SHEHZADI, S.A., AHMED, M.N., SIDDIQ, M., 2020. Bis-Schiff bases of 2,2′-dibromobenzidine as efficient corrosion inhibitors for mild steel in acidic medium. RSC Adv 10, 4499–4511. https://doi.org/10.1039/c9ra06443e

BAHAA EL-DIEN, M.E.G., ATWA, S.T., AHMED, A.A., EL-ETRE, A.Y., 2019. Synthesis and Characterization of Carbon Steel Corrosion Inhibitors Based on 4,5,6,7-tetrahydrobenzo-[b]thiophene Scaffold. Protection of Metals and Physical Chemistry of Surfaces 55, 179–186. https://doi.org/10.1134/S2070205119010106

CHEN, S., XU, M., TANG, Q., YANG, Z., TAN, X., HE, B., HUANG, J., 2021. A Theoretical Study of Some Schiff Bases as 304 Stainless Steel Inhibitors in HCl Solution. Int J Electrochem Sci 16, 1–11. https://doi.org/10.20964/2021.03.06

GAO, G., LIANG, C., 2007. Electrochemical and DFT studies of β-amino-alcohols as corrosion inhibitors for brass. Electrochim Acta 52, 4554–4559. https://doi.org/10.1016/j.electacta.2006.12.058

HASHEMI, A., MOJTABA NASR-ESFAHANI, BAKHSHESHI-RAD, H.R., 2021. Corrosion Inhibitive Property of Self-Assembled Films Formed by Schiff base Molecules on Carbon Steel Surface. Protection of Metals and Physical Chemistry of Surfaces 57, 849–857. https://doi.org-/10.1134/S2070205121040080

HEGAZY, M.A., HASAN, A.M., EMARA, M.M., BAKR, M.F., YOUSSEF, A.H., 2012. Evaluating four synthesized Schiff bases as corrosion inhibitors on the carbon steel in 1M hydrochloric acid. Corros Sci 65, 67–76. https://doi.org/10.1016/j.corsci.2012.08.005

HEGAZY, M.A., RASHWAN, S.M., MELEEK, S., KAMEL, M.M., 2021. Synthesis, characterization and mitigation action of innovative Schiff base on steel disintegration in sulfuric acid solution. Mater Chem Phys 267. https://doi.org/10.1016/j.matchemphys.2021.124697

HMAMOU, D. BEN, SALGHI, R., ZARROUK, A., BENALI, O., FADEL, F., ZARROK, H., HAMMOUTI, B., 2012. Carob seed oil: an efficient inhibitor of C38 steel corrosion in hydrochloric acid. International Journal of Industrial Chemistry 3, 1–9. https://doi.org/10.1186/2228-5547-3-25

JAFARI, H., AKBARZADE, K., DANAEE, I., 2019. Corrosion inhibition of carbon steel immersed in a 1 M HCl solution using benzothiazole derivatives. Arabian Journal of Chemistry. https://doi.org/10.1016/j.arabjc.2014.11.018

JAMIL, D.M., AL-OKBI, A.K., AL-BAGHDADI, S.B., AL-AMIERY, A.A., KADHIM, A., GAAZ, T.S., KADHUM, A.A.H., MOHAMAD, A.B., 2018. Experimental and theoretical studies of Schiff bases as corrosion inhibitors. Chem Cent J 12. https://doi.org/10.1186/s13065-018-0376-7

KAABI, I., DOUADI, T., DAOUD, D., ISSAADI, S., SIBOUS, L., CHAFAA, S., 2021. Synthesis, characterization and anti-corrosion properties of two new Schiff bases derived from diamino diphenyl ether on carbon steel X48 in 1M HCl. J Adhes Sci Technol 35, 559–589. https://doi.org/10.1080/01694243.2020.1816777

KAMEL, M.M., RASHWAN, S.M., MAHMOUD, M.A.A., EL-MEKAWY, S.A.A., AWAD, M.K., IBRAHIM, H.E., 2022a. Resorcinol Derivative as an Environmentally Friendly Low Carbon Steel Inhibitor in HCl Medium. ACS Omega 7, 17609–17619. https://doi.org/10.1021/acsomega.2c00153.

KAMEL, M., FOUDA, A. A., RASHWAN, S., MAREI, O. 2022b. 'Burghul Plant Extract as a Green Corrosion Inhibitor for Carbon Steel in Hydrochloric Acid Solution', Catrina: The International Journal of Environmental Sciences, 26(1), pp. 19-31. doi: 10.21608/cat.2022.277040.

KAUR, M., KAUR, K., KAUR, H., 2021. Quest of Schiff bases as corrosion inhibitors: A first principle approach. J Phys Org Chem 34. https://doi.org/10.1002/poc.4260

KHALED, M.A., ISMAIL, M.A., EL-HOSSIANY, A.A., FOUDA, A.E.A.S., 2021. Novel pyrimidine-bichalcophene derivatives as corrosion inhibitors for copper in 1 M nitric acid solution. RSC Adv 11, 25314–25333. https://doi.org/10.1039/d1ra03603c

KOOPMANS, T. (1934) über die Zuordnung von Wellenfunktionen und Eigenwerten zu den Einzelnen Elektronen Eines Atoms. Physica, 1, 104-113. https://doi.org/10.1016/S00318914(34)-90011-2.

KUMAR, S., KATYAL, P., CHAUDHARY, R.N., SINGH, V., 2022. Assessment of factors influencing bio-corrosion of magnesium-based alloy implants: A review. Mater Today Proc 56, 2680–2689. https://doi.org/10.1016/j.matpr.2021.09.262

KUMARI, P., LAVANYA, M., 2021. Optimization of Inhibition Efficiency of a Schiff Base on Mild Steel in Acid Medium: Electrochemical and RSM Approach. J Bio Tribocorros 7. https://doi.org/10.1007/s40735-021-00542-3.

LIANG, C., LIU, Z., LIANG, Q., HAN, G.C., HAN, J., ZHANG, S., FENG, X.Z., 2019. Synthesis of 2-aminofluorene bis-Schiff base and corrosion inhibition performance for carbon steel in HCl. J Mol Liq 277, 330-340. https://doi.org/10.1016/j.molliq.2018.12.095

NABATIPOUR, S., MOHAMMADI, S., MOHAMMADI, A., 2020. Synthesis and compa-rison of two chromone based Schiff bases containing methoxy and acetamido substitutes as highly sustainable corrosion inhibitors for steel in hydrochloric acid. J Mol Struct 1217. https://doi.org/10.1016/j.molstruc.2020.128367

NATASH MARY, R., NAZARETH, R., SUCHETAN, P.A., POTLA, K., 2022. Schiff Bases Derived from Triazoles as Corrosion Inhibitors for Maraging Steel in Acid Mixtures: Experimental and Theoretical Studies. Polycycl Aromat Compd 1–22. https://doi.org/10.1080/10406638.2022.2055582

NAZIR, U., AKHTER, Z., JANJUA, N.K., ADEEL ASGHAR, M., KANWAL, S., BUTT, T.M., SANI, A., LIAQAT, F., HUSSAIN, R., SHAH, F.U., 2020a. Biferrocenyl Schiff bases as efficient corrosion inhibitors for an aluminium alloy in HCl solution: A combined experimental and theoretical study. RSC Adv 10, 7585–7599. https://doi.org/10.1039/c9ra10692h

NAZIR, U., AKHTER, Z., JANJUA, N.K., ADEEL ASGHAR, M., KANWAL, S., BUTT, T.M., SANI, A., LIAQAT, F., HUSSAIN, R., SHAH, F.U., 2020. Biferrocenyl Schiff bases as efficient corrosion inhibitors for an aluminium alloy in HCl solution: A combined experimental and theoretical study. RSC Adv 10, 7585–7599. https://doi.org/10.1039/c9ra10692h

NEGM, N.A., MIGAHED, M.A., FARAG, R.K., FADDA, A.A., AWAD, M.K., SHABAN, M.M., 2018. High performance corrosion inhibition of novel tricationic surfactants on carbon steel in formation water: Electrochemical and computational evaluations. J Mol Liq 262, 363–375. https://doi.org/10.1016/j.molliq.2018.04.092

NJONG, R.N., NDOSIRI, B.N., NFOR, E.N., OFFIONG, O.E., 2018. Corrosion Inhibitory Studies of Novel Schiff Bases Derived from Hydralazine Hydrochloride on Mild Steel in Acidic Media. Open J Phys Chem 08, 15–32. https://doi.org/10.4236/ojpc.2018.81002

OLASUNKANMI, L.O., OBOT, I.B., EBENSO, E.E., 2016. Adsorption and corrosion inhibition properties of: N -{ n -[1-R-5-(quinoxalin-6-yl)-4,5-dihydropyrazol-3-yl]phenyl}methanesulfonamides on mild steel in 1 M HCl: Experimental and theoretical studies. RSC Adv 6, 86782–86797. https://doi.org/10.1039/c6ra11373g

SHAHABI, S., HAMIDI, S., GHASEMI, J.B., NOROUZI, P., SHAKERI, A., 2019. Synthesis, experimental, quantum chemical and molecular dynamics study of carbon steel corrosion inhibition

effect of two Schiff bases in HCl solution. J Mol Liq 285, 626–639. https://doi.org/10.10-16/j.molliq.2019.04.137

Tang, Z., 2019. A review of corrosion inhibitors for rust preventative fluids. Curr Opin Solid State Mater Sci. https://doi.org/10.1016/j.cossms.2019.06.003

VERMA, C., EBENSO, E.E., QURAISHI, M.A., 2017. Corrosion inhibitors for ferrous and non-ferrous metals and alloys in ionic sodium chloride solutions: A review. J Mol Liq. https://doi.org/10.1016/j.molliq.2017.10.094

VERMA, C., OLASUNKANMI, L.O., EBENSO, E.E., QURAISHI, M.A., OBOT, I.B., 2016. Adsorption Behavior of Glucosamine-Based, Pyrimidine-Fused Heterocycles as Green Corrosion Inhibitors for Mild Steel: Experimental and Theoretical Studies. Journal of Physical Chemistry C 120, 11598–11611. https://doi.org/10.1021/acs.jpcc.6b04429

WANG, X., XIANG JAINI , HUANG ZONGGUAN 2021 Study on the Corrosion Inhibition Performance of a Schiff Base for Carbon Steel in 1 M HCl Solution. Int J Electrochem Sci ArticleID:210916. https://doi.org/10.20964/2021.09.36

ZHANG, D.Q., GAO, L.X., ZHOU, G.D., 2004. Inhibition of copper corrosion in aerated hydrochloric acid solution by heterocyclic compounds containing a mercapto group. Corros Sci 46, 3031–3040. https://doi.org/10.1016/j.-corsci.2004.04.012

ZHANG, Q.H., HOU, B.S., XU, N., XIONG, W., LIU, H.F., ZHANG, G.A., 2019. Effective inhibition on the corrosion of X65 carbon steel in the oilfield produced water by two Schiff bases. J Mol Liq 285, 223–236. https://doi.org/10.1016/j.molliq.2019.04.072

ZHUANG, W., WANG, X., ZHU, W., ZHANG, Y., SUN, D., ZHANG, R., WU, C., 2021. Imidazoline Gemini Surfactants as Corrosion Inhibitors for Carbon Steel X70 in NaCl Solution. ACS Omega 6, 5653–5660. https://doi.org/10.1021/acsomega.0c06103.

النهج التجريبي والنظري باستخدام قاعدة شيف كمثبط للتآكل للفولاذ الكربوني في وسط حمضي

أمل رفعت التهامي[1], مدحت كامل [1]، احمد ابو المجد[1] ,صلاح رشوان[1] , عبدالعزيز فودة [2]، محمد عوض[3]، فاتن أطلام[3]

[1]كلية العلوم، قسم الكيمياء، جامعة قناة السويس، مصر

[2]كلية العلوم، قسم الكيمياء، جامعة المنصورة، مصر

[3]كلية العلوم، قسم الكيمياء، جامعة طنطا، مصر

الملخص العربي

التآكل هو تدمير لخصائص المادة بسبب تفاعل كهروكيميائي أو كيميائي مع البيئة المحيطة. لذلك يحاول الباحثون فهم هذه الظاهرة لحل هذه المشكلة. في هذا البحث تم دراسة حركية التآكل وتثبيط التآكل للصلب الكربونى في تركيز نصف مولار من حمض الهيدروكلوريك في غياب و وجود تركيزات مختلفة من أحد مركبات قواعد شيف. وبحساب كفاءة هذا المركب لتثبيط تآكل الصلب الكربوني بواسطة الطرق الكيميائية و الكهروكيميائية المختلفة مثل الاستقطاب الجهدي الحركي - طيف المعاوقة الكهروكيميائية و طريقة فقدان الوزن عند درجات حرارة من 298-333 كلفن .واثبتت النتائج ان معدل التآكل للصلب الكربوني يقل مع زيادة تركيز مركب الشيف وبالتالي تزيد كفاءة التثبيط حتى تصل لأقصى قيمة (84%). يشير الاختلاف فى الخصائص الحركية والديناميكية الحرارية لمركب الشيف على سطح الصلب الكربونى الى امتزاز مختلط (كيميائى وفيزيائى). تشير منحنيات الاستقطاب الى النوع المختلط من نشاط التثبيط متبوعا بنموذج لانجمير. النتائج التجريبية مدعومة بنظرية الكثافة الوظيفية ومحاكاة مونت كارلو، مما يشير إلى سلوك تثبيط التآكل لمركب الشيف على سطح الصلب الكربونى فى البيئات الحمضية. كشف تحليل SEM, EDX عن تغطية المثبط لسطح الصلب الكربوني عن طريق عملية الادمصاص. دعمت الخصائص الكمية فعالية تثبيط مركب الشيف.

.